

# Germanium wrap-around photodetectors on Silicon photonics

Ryan Going,<sup>1†</sup> Tae Joon Seok,<sup>1†</sup> Jodi Loo,<sup>1</sup> Kyle Hsu,<sup>1</sup> and Ming C. Wu<sup>1\*</sup>

<sup>1</sup>Department of Electrical Engineering and Computer Sciences, University of California, Berkeley, CA 94720, USA

<sup>†</sup>These authors contributed equally.

\*wu@eecs.berkeley.edu

**Abstract:** We present a novel waveguide coupling scheme where a germanium diode grown via rapid melt growth is wrapped around a silicon waveguide. A 4 fF PIN photodiode is demonstrated with 0.95 A/W responsivity at 1550 nm, 6 nA dark current, and nearly 9 GHz bandwidth. Devices with shorter intrinsic region exhibit higher bandwidth (30 GHz) and slightly lower responsivity (0.7 A/W). An NPN phototransistor is also demonstrated using the same design with 14 GHz  $f_T$ .

©2015 Optical Society of America

**OCIS codes:** (230.0230) Optical devices; (230.5160) Photodetectors; (230.5170) Photodiodes.

---

## References and links

1. D. A. B. Miller, "Device requirements for optical interconnects to silicon chips," *Proc. IEEE* **97**(7), 1166–1185 (2009).
2. S. Manipatruni, M. Lipson, and I. A. Young, "Device scaling considerations for nanophotonic CMOS global interconnects," *IEEE J. Sel. Top. Quantum Electron.* **19**(2), 8200109 (2013).
3. C. T. DeRose, D. C. Trotter, W. A. Zortman, A. L. Starbuck, M. Fisher, M. R. Watts, and P. S. Davids, "Ultra compact 45 GHz CMOS compatible Germanium waveguide photodiode with low dark current," *Opt. Express* **19**(25), 24897–24904 (2011).
4. L. Chen and M. Lipson, "Ultra-low capacitance and high speed germanium photodetectors on silicon," *Opt. Express* **17**(10), 7901–7906 (2009).
5. C.-K. Tseng, W.-T. Chen, K.-H. Chen, H.-D. Liu, Y. Kang, N. Na, and M.-C. M. Lee, "A self-assembled microbonded germanium/silicon heterojunction photodiode for 25 Gb/s high-speed optical interconnects," *Sci. Rep.* **3**, 3225 (2013).
6. L. Vivien, A. Polzer, D. Marris-Morini, J. Osmond, J.-M. Hartmann, P. Crozat, E. Cassan, C. Kopp, H. Zimmermann, and J.-M. Fédéli, "Zero-bias 40Gbit/s germanium waveguide photodetector on silicon," *Opt. Express* **20**(2), 1096–1101 (2012).
7. S. Assefa, F. Xia, and Y. A. Vlasov, "Reinventing Germanium avalanche photodetector for nanophotonic on-chip optical interconnects," *Nature* **464**(7285), 80–84 (2010).
8. N.-N. Feng, P. Dong, D. Zheng, S. Liao, H. Liang, R. Shafiiha, D. Feng, G. Li, J. E. Cunningham, A. V. Krishnamoorthy, and M. Asghari, "Vertical p-i-n germanium photodetector with high external responsivity integrated with large core Si waveguides," *Opt. Express* **18**(1), 96–101 (2010).
9. D. Feng, S. Liao, P. Dong, N.-N. Feng, H. Liang, D. Zheng, C.-C. Kung, J. Fong, R. Shafiiha, J. Cunningham, A. V. Krishnamoorthy, and M. Asghari, "High-speed Ge photodetector monolithically integrated with large cross-section silicon-on-insulator waveguide," *Appl. Phys. Lett.* **95**(26), 261105 (2009).
10. T. Yin, R. Cohen, M. M. Morse, G. Sarid, Y. Chetrit, D. Rubin, and M. J. Paniccia, "31 GHz Ge n-i-p waveguide photodetectors on Silicon-on-Insulator substrate," *Opt. Express* **15**(21), 13965–13971 (2007).
11. Y. Zhang, S. Yang, Y. Yang, M. Gould, N. Ophir, A. E.-J. Lim, G.-Q. Lo, P. Magill, K. Bergman, T. Baehr-Jones, and M. Hochberg, "A high-responsivity photodetector absent metal-germanium direct contact," *Opt. Express* **22**(9), 11367–11375 (2014).
12. L. Virost, P. Crozat, J.-M. Fédéli, J.-M. Hartmann, D. Marris-Morini, E. Cassan, F. Boeuf, and L. Vivien, "Germanium avalanche receiver for low power interconnects," *Nat. Commun.* **5**, 4957 (2014).
13. D. Hisamoto, W.-C. Lee, J. Kedzierski, H. Takeuchi, K. Asano, C. Kuo, E. Anderson, T.-J. King, J. Bokor, and C. Hu, "FinFET—a self-aligned double-gate MOSFET scalable to 20 nm," *IEEE Trans. Electron. Dev.* **47**(12), 2320–2325 (2000).
14. Y. Liu, M. Deal, and J. Plummer, "Rapid melt growth of Germanium crystals with self-aligned microcrucibles on Si substrates," *J. Electrochem. Soc.* **152**(8), G688–G693 (2005).
15. J. Feng, G. Thareja, M. Kobayashi, S. Chen, A. Poon, Y. Bai, P. B. Griffin, S. S. Wong, Y. Nishi, and J. D. Plummer, "High-performance gate-all-around GeOI p-MOSFETs fabricated by rapid melt growth using plasma nitridation and ALD gate dielectric and self-aligned NiGe contacts," *IEEE Electron Device Lett.* **29**(7), 805–807 (2008).

16. Y. Liu, K. Gopalakrishnan, P. B. Griffin, K. Ma, M. D. Deal, and J. D. Plummer, "MOSFETs and high-speed photodetectors on Ge-on-insulator substrates fabricated using rapid melt growth," Electron Devices Meeting, 2004. IEDM Technical Digest. IEEE International 1001–1004 (2004).
  17. S. Assefa, F. Xia, S. W. Bedell, Y. Zhang, T. Topuria, P. M. Rice, and Y. A. Vlasov, "CMOS-integrated high-speed MSM Germanium waveguide photodetector," Opt. Express **18**(5), 4986–4999 (2010).
  18. R. W. Going, J. Loo, T.-J. King Liu, and M. C. Wu, "Germanium gate PhotoMOSFET integrated to silicon photonics," IEEE J. Sel. Top. Quantum Electron. **20**(4), 8201607 (2014).
  19. D. Taillaert, F. Van Laere, M. Ayre, W. Bogaerts, D. van Thourhout, P. Bienstman, and R. Baets, "Grating couplers for coupling between optical fibers and nanophotonic waveguides," Jpn. J. Appl. Phys. **45**(8A), 6071–6077 (2006).
  20. M. Takenaka, K. Morii, M. Sugiyama, Y. Nakano, and S. Takagi, "Dark current reduction of Ge photodetector by GeO<sub>2</sub> surface passivation and gas-phase doping," Opt. Express **20**(8), 8718–8725 (2012).
  21. L. Vivien, J. Osmond, J.-M. Fédéli, D. Marris-Morini, P. Crozat, J.-F. Damlencourt, E. Cassan, Y. Lecunff, and S. Laval, "42 GHz p.i.n Germanium photodetector integrated in a silicon-on-insulator waveguide," Opt. Express **17**(8), 6252–6257 (2009).
  22. C. L. Claeys and E. Simoen, *Germanium-Based Technologies* (Elsevier, 2007).
  23. S. M. Sze and K. K. Ng, *Physics of Semiconductor Devices*, 3rd ed. (John Wiley & Sons, 2007).
  24. K.-W. Ang, M.-B. Yu, G.-Q. Lo, and D.-L. Kwong, "Low-voltage and high-responsivity germanium bipolar phototransistor for optical detections in the near-infrared regime," IEEE Electron Device Lett. **29**(10), 1124–1127 (2008).
- 

## 1. Introduction

Low energy per bit optical interconnects offer much promise for reducing power consumption in communications [1,2] and creating highly sensitive receivers is essential for that. Creating low-capacitance photodiodes tightly integrated to receiver electronics can satisfy this requirement.

Several groups in recent years have focused on creating low-capacitance, high-speed, and high-responsivity germanium photodiodes on silicon waveguides [3–12]. These diodes couple to the waveguide either evanescently, sitting on top of the waveguide, or butt-coupled to the end of a terminated waveguide. An alternative that has yet to be explored is a combination of these two coupling schemes, where the photodiode wraps-around the silicon waveguide coupling light evanescently from all sides of the waveguide, much like the wrap-around gate of the finFET [13].

Recently, rapid melt growth (RMG) was developed to provide single crystal germanium on oxide using a silicon seed [14], and also has the ability to produce single crystalline germanium which conformally coats the oxidized substrate. It has so far been demonstrated for high mobility FET channels [15], photodiodes [5,16,17], and phototransistors [18]. We use RMG to demonstrate a germanium photodiode with 0.95 A/W responsivity at 1550 nm, 6 nA of dark current at  $-1$  V and up to a 9 GHz bandwidth, with less than 4 fF of capacitance. By narrowing the intrinsic region slightly, and taking a small hit in the responsivity (0.7 A/W) the bandwidth increases to over 30 GHz. Additionally we utilize the same design to demonstrate a 14 GHz NPN phototransistor with upwards of 14 A/W responsivity.

## 2. Photodiode design and fabrication

The basic design imagines a lateral PIN photodiode where the intrinsic region is 'wrapped' around a single mode silicon waveguide. The central idea being that the germanium will absorb the light from the waveguide evanescently over its length, and by moving the contacts away from the optical mode, overall quantum efficiency will be improved. Due to relying on evanescent coupling, this particular arrangement also allows the photodiode itself to be very thin, reducing the overall capacitance in a lateral junction arrangement. Because this geometry requires non-planar germanium, rapid melt growth was chosen as the growth technique.

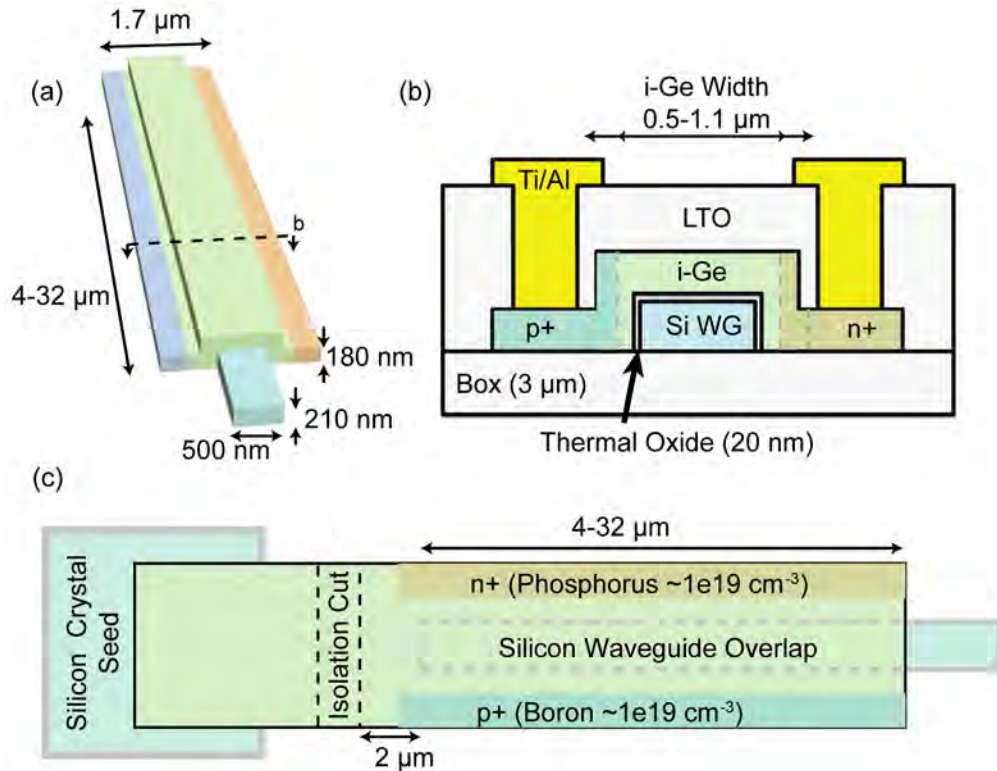


Fig. 1. (a) 3D schematic of the wrap-around photodiode design. (b) A cross-section of the wrap-around photodiode showing the lateral doping scheme. (c) Top-down view of the photodiode (not-to-scale) showing the silicon seed for RMG, the cut in the Ge performed to isolate the diode from the seed, and the amount of waveguide overlap.

The specific photodiode design is depicted in Fig. 1, where a 3D overview of the device is shown in Fig. 1(a), and a cross section is shown in Fig. 1(b). This shows the germanium layer, 180 nm thick, to wrap-around an etched silicon layer (210 x 500 nm) on the 3 μm buried oxide (BOX) layer for optical and electrical isolation. The silicon layer has a thin oxide grown between it and the germanium as part of the RMG process and for electrical isolation from the waveguide. The silicon layer serves as a single mode optical waveguide, and also contains grating couplers for coupling onto the chip from single mode optical fiber.

The lateral doping scheme is shown with p + and n + regions away from the waveguide with only intrinsic germanium immediately surrounding the waveguide. The rationale for this design is to move the highly doped regions and metal contacts away from the areas of the photodiode where the optical mode will be present in order to reduce free carrier absorption and slow carrier diffusion from heavily doped regions as well as scattering from metal contacts.

The devices were fabricated by first depositing and patterning a thin (140 nm) layer of low stress silicon nitride as a hard mask. A shallow dry etch (70 nm) was performed for the rectangular grating couplers which were given a 630 nm pitch with 50% duty cycle for good coupling at 1550 nm [19]. Next the patterned silicon was dry-etched down to the BOX layer to isolate the waveguides and crystal seed areas. A thin thermal oxide (20 nm) was grown both to smooth the waveguide sidewalls and to isolate the germanium from the silicon for the RMG step. A small opening was wet etched in the oxide at the crystal seed locations to expose the underlying silicon without damage. Next 180 nm of Germanium was deposited via low pressure chemical vapor deposition (LPCVD) with a 5 nm Silicon wetting layer for

stiction to the oxide. The germanium was patterned and dry-etched. A cleaning step was performed where the germanium was protected while the wafer was submerged in hot peroxide followed by a quick HF dip to remove any remaining germanium from waveguide sidewalls. This was followed by a 400 nm coating of low-temperature oxide (LTO).

The wafer was placed in a rapid thermal annealer, where the temperature was quickly ramped to 1050 °C for 1 second, and then immediately cooled as in previous RMG papers [14,17,18]. Contact holes were dry etched into the LTO down to the germanium, and then separate boron ( $10^{15}$  cm<sup>-2</sup> dose, 25 keV energy) and phosphorus ( $10^{15}$  cm<sup>-2</sup> dose, 15 keV energy) implants were performed for p and n-type doping respectively. The dopants were activated with a 5 minute anneal at 450 °C. The low temperature is to ensure very low phosphorus diffusion [22], and no further annealing is performed. Finally, a Ti/Al metal stack (50 nm/450 nm) was sputtered and then dry-etched to form electrical contacts. The metal etch also performs the isolation cut by over-etching through germanium exposed when opening the contact vias.

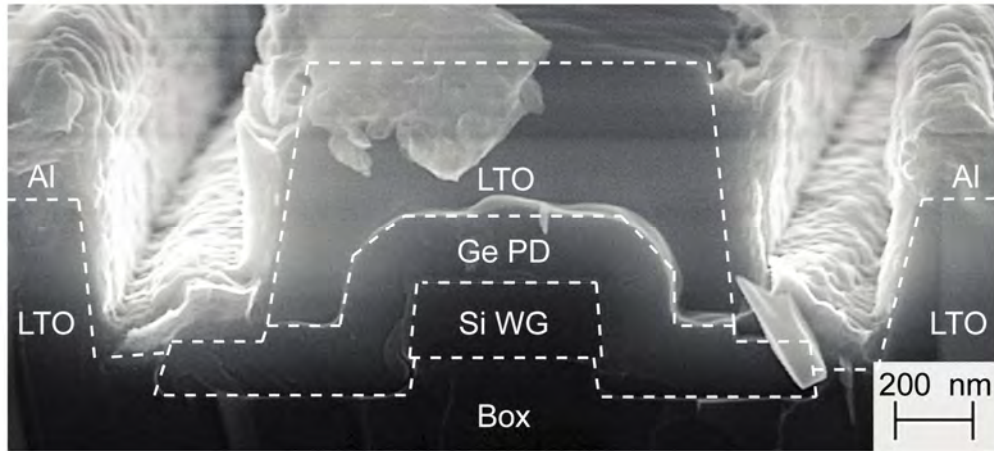


Fig. 2. Scanning electron microscope (SEM) cross-section of a completed photodiode. The image has had different sections of the device highlighted for clarity.

The resulting device can be seen in Fig. 2, which shows a scanning electron micrograph (SEM) cross-section of a cleaved device. The resulting germanium is smooth, and cleanly wraps-around the silicon waveguide with a thin oxide between the two. There is evidence over-etching both in the silicon full-etch step and in the oxide-etching step. One result shows a germanium device, which actually wraps slightly below the plane of the waveguide, which could improve the optical coupling. However, the over-etching into the germanium can degrade performance by introducing significant dark current from increased surface leakage currents [20]. Both of these will be discussed in more detail with the measurement results.

### 3. Photodiode results and discussion

#### 3.1 DC and optical measurements

To measure the responsivity of the photodiodes, light was coupled into the waveguide by a single mode optical fiber, which was part of a fiber array. On the ends of the waveguide array were grating couplers connected with a short length of waveguide for optical alignment purposes. This structure also gave us the insertion loss of a single grating coupler and waveguide, which at 1550 nm was determined to be -7.1 dB. The current-vs-voltage (I-V) measurements were made using an HP4145B semiconductor parameter analyzer. An HP 4284A LCR meter was used to measure capacitance as a function of voltage at 1 MHz.

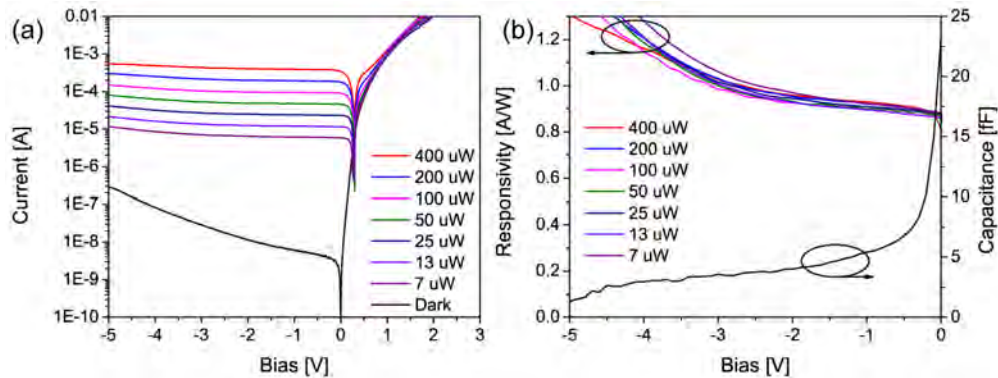


Fig. 3. (a) Current vs bias for a 16  $\mu\text{m}$  overlap length photodiode showing dark current and differing amounts of photocurrent with different optical powers. (b) Extracted responsivity vs bias for the same diode as well as the measured capacitance.

As an example, we present a diode with 16  $\mu\text{m}$  of waveguide overlap, giving a total length of 18  $\mu\text{m}$ , which has the I-V curve shown in Fig. 3(a). It can be seen that this diode has extremely low dark current of 6 nA at  $-1$  V reverse bias, and only 300 nA at  $-5$  V. At  $-1$  V this corresponds to less than  $200 \text{ mA/cm}^2$  of dark current density, which is comparable to germanium diodes made with more traditional epitaxy methods [6,21]. Figure 3(b) shows the responsivity is largely flat up to  $-3$  V, and begins to rise quickly with larger bias. One possibility is the onset of avalanche gain at 3 to 4 V reverse bias due to device simulations showing localized electric fields in excess of the ionization threshold [22] near the heavily doped n + junction. The capacitance quickly drops with a small bias indicating the diodes are initially not fully depleted at 0 V.

The wrap-around structure was simulated with finite difference time domain (FDTD) software to calculate the mode overlap and expected responsivity, assuming collection of all generated photocarriers. The electric energy distribution can be seen in Fig. 4(a), which shows a cross-section of the wrap-around structure. What can be immediately seen from the distribution is that the majority of the energy in the germanium is centered above the silicon waveguide, with relatively little energy in the side lobes of the germanium. A large portion of the energy is also in the germanium itself, due to the strong evanescent coupling into the germanium from the silicon waveguide, helped by the higher refractive index of germanium compared to silicon. All of this implies that a majority of the light should be absorbed by the germanium in a relatively short coupling length, and additionally, the majority of the light will be absorbed in the center of the germanium structure, which is where we have placed the i-Ge portion of the diode.

Additionally, the FDTD simulations were performed to extract the responsivity of the photodiode with respect to the waveguide overlap length. This calculation only accounts for the absorption in the i-Ge region of the diode, assuming that light absorbed in the heavily doped p and n-type contact regions will not be collected due to quick recombination. The simulated responsivity can be seen in Fig. 4(b). Several different length photodiodes were fabricated and measured against the FDTD calculations. In this case the length mentioned refers to the amount of overlap with the silicon waveguide, while all diodes were fabricated with an additional 2  $\mu\text{m}$  of Germanium after the end of the waveguide to ensure the waveguide would not extend past the Germanium due to lithographic alignment error. Thus the 32  $\mu\text{m}$  diode has 32  $\mu\text{m}$  of overlap with the silicon waveguide and 34  $\mu\text{m}$  of total length.

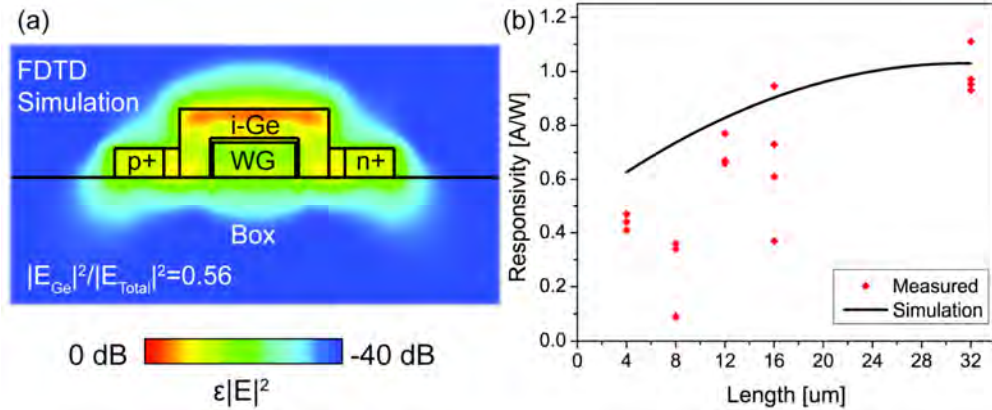


Fig. 4. (a) FDTD simulation of the wrap-around structure. (b) Responsivity at 1550 nm versus waveguide overlap length for both measured photodiode devices and simulated devices.

For the responsivity measured in Fig. 4(b) a reverse bias of  $-2$  V was applied to the photodiode. Other than the  $8$   $\mu\text{m}$  photodiodes, there is good agreement between measurement and FDTD calculations, with the  $4$   $\mu\text{m}$  diodes demonstrating responsivity near  $0.5$  A/W, and the  $32$   $\mu\text{m}$  diodes with responsivities near  $1$  A/W. The  $8$ ,  $12$ , and  $16$   $\mu\text{m}$  diodes show more considerable variation among themselves, and with the FDTD values. One possibility is that the FDTD results at those lengths range show some resonant effects. The absorption at a resonant length for a fabricated device would be highly dependent on the quality of the sidewalls which is likely highly variable from device to device, resulting in drastically different measured responsivities. It is also possible some variability in measured responsivity comes from variation in material quality as some diodes had notably higher dark current, on the order of several  $\mu\text{A}$ . However these results demonstrate photodiodes with  $0.8$  A/W responsivity or better with just  $12$   $\mu\text{m}$  of waveguide overlap, which means high responsivity with compact design.

### 3.2 Photodiode RF response

Additionally we obtained the high frequency response of the wrap around photodiode using a network analyzer and measured the  $S_{21}$  of the photodiode. The parameter network analyzer (PNA) drove a  $40$  GHz EO Space intensity modulator with port 1, which was biased to the  $3$  dB point of the modulator. A fiber laser was input to the modulator, the output of which went to a single mode fiber probe that coupled to the chip under test via grating coupler. The photodiode was then probed with a ground-signal RF probe, which fed into port 2 of the PNA. The DC bias was applied through the PNA. The measurement was calibrated using a commercial  $70$  GHz fiber coupled photodiode. The average optical power during the measurements incident on the photodiode was  $100$   $\mu\text{W}$ . There was some impedance mismatch between the probe and the photodiode under test causing ripples in the  $S_{21}$  spectra, which was compensated in post-processing by isolating the ripples common to all spectra and subtracting them as in Ref [7].

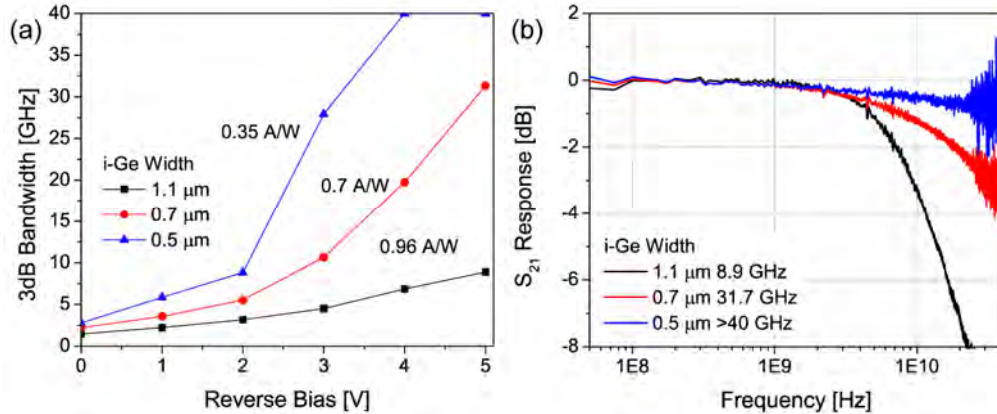


Fig. 5. (a) The measured 3dB bandwidth of three photodiodes with differing i-Ge with and (b) their respective  $S_{21}$  spectra at highest measured bandwidth, which include a 5-point box smooth.

To examine the effects of transit speed limited bandwidth, several photodiodes were produced with different i-Ge widths. The designed separation was 1.1  $\mu\text{m}$ , which was present in all of the previously presented diodes. Additionally, two narrower diodes were produced with 0.7  $\mu\text{m}$  and 0.5  $\mu\text{m}$  i-Ge widths, which should have higher bandwidths and are seen in Fig. 5. All of these splits were done on 32  $\mu\text{m}$  length photodiodes, though the previously described 16  $\mu\text{m}$  diode was also measured and its bandwidth is comparable to those presented here. It can be seen in Fig. 5(a) that for the standard photodiode design, the bandwidth at  $-5$  V of reverse bias is almost 9 GHz, and that the speed is almost saturated at that point. Because of the wrap-around geometry, the total distance a carrier would travel from one contact to the other is nearly 2  $\mu\text{m}$ . Assuming velocity saturation of  $6 \times 10^6$  cm/s the expected 3dB bandwidth would be 13.5 GHz, so the results are quite close. However, at lower voltages the bandwidth is considerably lower. In fact based on the width and that the carriers in Germanium saturate at an electric field of  $10^4$  V/cm, there should be velocity saturation at about  $-2$  V. Device simulations show that with a background p-type concentration of  $10^{16}$   $\text{cm}^{-3}$  a 5 V bias would be needed to reach uniform electric fields sufficient for carrier velocity saturation to reach the full bandwidth.

However, this is not a fundamental limitation as evidenced by the devices with narrower i-Ge regions in Fig. 5. Because the capacitance is so low, the bandwidth of all of these photodiodes is expected to be transit time limited. By nearly halving the i-Ge width, and thus decreasing the carrier transit distance, the bandwidth more than doubles to 31 GHz at  $-5$  V, and by reducing further to 0.5  $\mu\text{m}$ , the bandwidth increases to over 40 GHz. In fact due to the limited bandwidth of the modulator in the test setup, the ultimate bandwidth of the 0.5  $\mu\text{m}$  wide device could not be measured, but it can be seen that at  $-5$  V bias, at 40 GHz there is only a 1 dB drop in the  $S_{21}$ . There is a trade-off naturally for increasing the speed in this manner, which is that because the i-Ge region is narrower, the responsivity is reduced. Figure 5(a) also shows the average responsivity values for several devices of a given i-Ge width. However, because of the specific optical mode profile the drop in responsivity is not proportional to the reduction in i-Ge width, and so a trade-off can be made between responsivity and desired bandwidth.

#### 4. NPN phototransistor

##### 4.1 Phototransistor design using wrap-around photodiode process

As mentioned earlier, having a low-capacitance photodiode is not the end of the story, and in fact the other half is to bring the photodiode extremely close to the first transistor in the

amplifying receiver. Here we demonstrate that using the same process as that of the wrap-around photodiode, an NPN phototransistor with high  $f_T$  can be produced. Figure 6 shows the basic design of the device, which is geometrically identical to the wrap-around photodiode, meaning it should share the same strong optical coupling to the waveguide. The primary difference is that instead of creating a PIN photodiode with a separate p and n-implant on either side of the device, the NPN simply implants n-type dopants (phosphorus) on both ends while leaving the center of the device undoped. Because germanium is natively lightly p-type [22] the device will act as an n + p-n + transistor with a very long base. Additionally, to simplify the fabrication there is no base contact, making this a floating base phototransistor. Because of the very long, low-doped base, the device is expected to exhibit strong base-width modulation effects [23] but should be relatively fast. Additionally, the base is situated where the i-Ge is present in the PIN diode, meaning the majority of the light will be absorbed directly in the base, which is the preferred location for a phototransistor.

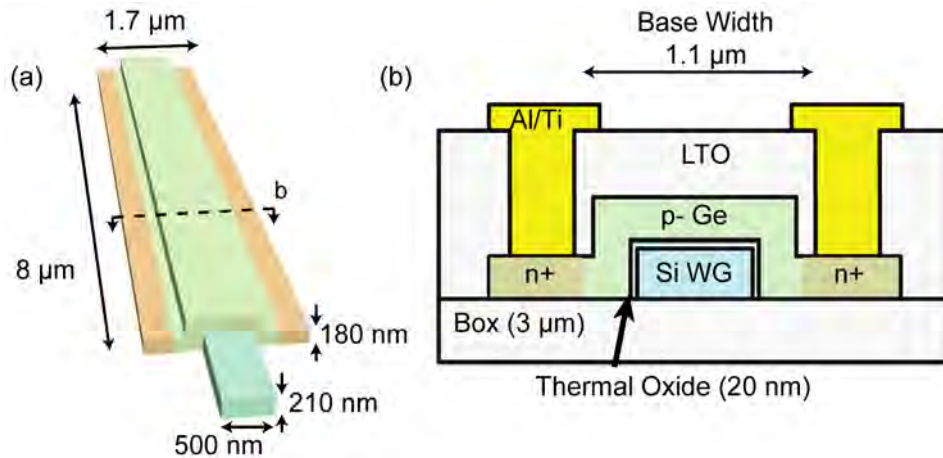


Fig. 6. (a) 3D schematic of the wrap-around NPN phototransistor with (b) cross section showing the doping scheme and emitter/collector contacts. The base is left floating.

#### 4.2 DC measurements of the NPN transistor

The NPN phototransistor was measured the same way as the PIN photodiode. Figure 7(a) shows the I-V measurement in both the dark state and with different amounts of optical excitation. Several key aspects of the operation can be seen from the I-V. Namely the large amount of dark current is seen at low voltages. This is likely due to the very-low doping of base, and is caused by punch-through [23]. Because the similarly structured and doped PIN diode was nearly fully depleted at  $-2$  V bias, we should expect punch-through to occur at a similar voltage in this NPN transistor. Beyond that voltage the dark current should begin to rise dramatically. However despite this the gain is still relatively high, and we see significant photocurrent on top of the dark current for relatively low optical powers. In fact in Fig. 7(b) the extracted responsivity and photocurrent gain can be seen to be quite high. At about 1.5 V bias, the gain peaks and begins to reduce, as a result of likely punch-through. To extract the photocurrent gain, one must know the underlying responsivity of the structure without gain. While there are identical 8  $\mu\text{m}$  PIN photodiodes on the wafer, many we measured had a wide variability in responsivity as discussed earlier. Thus to have a more conservative estimate of the gain we assume a 0.76 A/W responsivity which comes from the FDTD calculation of this structure. Thus it is entirely possible the device has a true photocurrent gain even higher than 18 with a 5  $\mu\text{W}$  input. However, the responsivity is a direct measurement, and so we confidently report a responsivity of nearly 14 A/W with a 5  $\mu\text{W}$  input at 1.5 V.

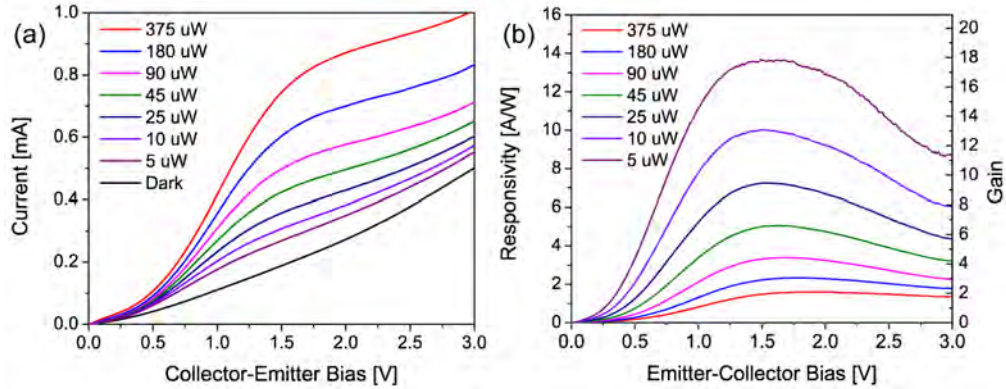


Fig. 7. (a) Shows the photo I-V response of an  $8\mu\text{m}$  phototransistor and (b) shows the extracted responsivity and photocurrent gain.

Another interesting phenomenon is that the gain decreases with increasing optical power. Because this is a floating base phototransistor, the optical power input to the device is equivalent to the base current bias applied to a traditional bipolar junction transistor (BJT). One would expect typically that an increase in base current might increase the gain, or at least have a relatively constant amount of gain. However because the base in this device has such low doping, by increasing the optical power, the generation rate in the base increases so much that the effective doping level in the base begins to increase as well. Since the doping level ratio between emitter and base is a large factor in the gain, reducing this ratio would reduce the gain. This effective increase in the base doping would also reduce base-width modulation effects and increase the voltage required for punch-through. This can be seen in Fig. 7(b) as a shift in the gain peak from 1 V to 1.5 V for increasing optical power.

#### 4.3 High frequency response of NPN phototransistor

The RF response of the NPN phototransistor was again measured identically to that of the PIN photodiode. In addition to the measurement of the  $S_{21}$  response, because the gain varied greatly with respect to input power, it is also interesting to examine the  $S_{21}$  versus optical input power. Additionally since we have already extracted the photocurrent gain for the device, we can actually construct an  $h_{21}$  plot, which is the  $S_{21}$  response normalized to the amount of gain present at DC. The  $f_T$  or unity gain frequency of the phototransistor is then the frequency at which the photocurrent gain is 1. This is typically a more useful metric for transistors than 3dB frequencies, though the latter is very important for receiver circuitry. The results are shown in Fig. 8, which shows that although gain reduces with increased optical power, the 3dB frequency actually increases with increasing optical bias. In fact we see that with  $5\mu\text{W}$  of optical bias, the transistor operates out to 14 GHz. This is considerably higher than the 7 GHz gain-bandwidth product most recently reported for a germanium photoBJT [24]. However at this optical power, the 3dB frequency is under 1 GHz while the gain is very high. While increasing the optical bias increases the 3dB frequency, it also reduces gain and  $f_T$  likely due to the Kirk effect [23]. By increasing the base doping during an additional background doping step, and reducing the base width, the transistor operation speed both  $f_T$  and the 3dB bandwidth will be dramatically improved making this a more practical device for modern communications speeds of 25 GB/s and higher. Additionally, to make the device more power efficient, it would be beneficial to add a base contact to provide the base current bias electrically rather than optically.

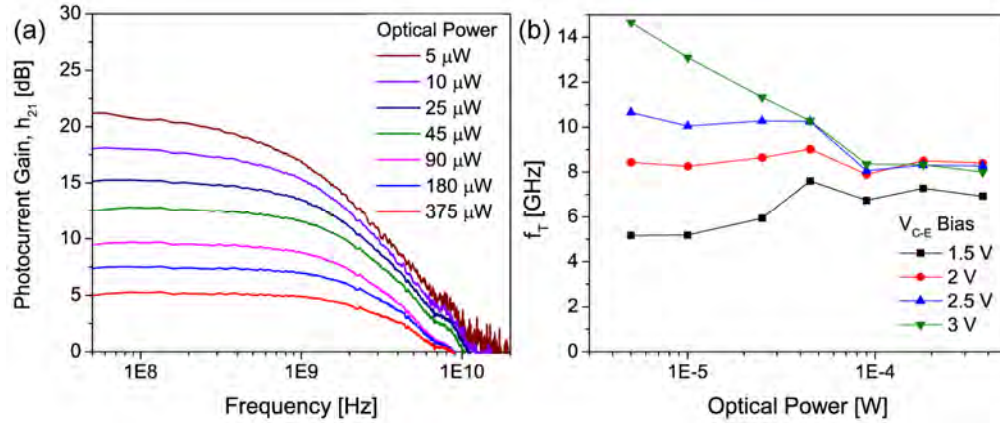


Fig. 8. (a)  $h_{21}$  frequency response of the 8 $\mu$ m NPN phototransistor measured with a 3V bias as a function of optical input power. (b) Measured  $f_T$  as a function of optical input power and collector-emitter bias.

## 5. Conclusions

In this paper, we demonstrate two novel devices using RMG germanium integrated on silicon photonics. The first is a 4 fF PIN photodiode with 6 nA of dark current and 0.95 A/W responsivity at 1550 nm. By varying the width of the intrinsic region we were able to measure 3 dB frequencies well over 40 GHz. The second device is an NPN phototransistor with 14 A/W responsivity when illuminated with only 5  $\mu$ W of 1550 nm light and a peak  $f_T$  of 14.5 GHz.

## Acknowledgments

We would like to acknowledge funding from E3S (NSF Award 0939514), CIAN (#EEC-0812072), Defense Advanced Research Projects Agency (DARPA) E-PHI program under Grant No. HR0011-11-2-0021, Intel, NSF Fellowship (DGE 1106400). We would also like to offer special thanks to Sangyoon Han, Phil Sandborn, Chris Keraly, and the Berkeley Nanolab.